

FAAH inhibitor URB597

Subjects: Cell Biology | Neurosciences

Contributor: Rita Businaro

Since the inhibition of fatty acid amide hydrolase (FAAH), the main catabolic enzyme of anandamide (AEA), may provide beneficial effects in mice model of Alzheimer's disease (AD)-like pathology, we aimed at determining whether the FAAH inhibitor URB597 might target microglia polarization and alter the cytoskeleton reorganization induced by the amyloid- β peptide ($A\beta$). The morphological evaluation showed that $A\beta$ treatment increased the surface area of BV-2 cells, which acquired a flat and polygonal morphology. URB597 treatment partially rescued the control phenotype of BV-2 cells when co-incubated with $A\beta$. Moreover, URB597 reduced both the increase of Rho protein activation in $A\beta$ -treated BV-2 cells and the $A\beta$ -induced migration of BV-2 cells, while an increase of Cdc42 protein activation was observed in all samples. URB597 also increased the number of BV-2 cells involved in phagocytosis. URB597 treatment induced the polarization of microglial cells towards an anti-inflammatory phenotype, as demonstrated by the decreased expression of iNOS and pro-inflammatory cytokines along with the parallel increase of Arg-1 and anti-inflammatory cytokines. Taken together, these data suggest that FAAH inhibition promotes cytoskeleton reorganization, regulates phagocytosis and cell migration processes, thus driving microglial polarization towards an anti-inflammatory phenotype.

Keywords: URB597 ; N-arachidonylethanolamine (AEA) ; fatty acid amide hydrolase (FAAH) ; microglia ; actin cytoskeleton ; cell migration ; M1/M2 phenotypes ; neuroinflammation

1. Introduction

Alzheimer's disease (AD) is a neurodegenerative disorder characterized by the progressive and inescapable cognitive deterioration, whose main neuropathological hallmarks are the formation of intracellular neurofibrillary tangles and extracellular senile plaques, producing synaptic dysfunction, and ultimately, neural death. While neurofibrillary tangles are composed of hyperphosphorylated tau protein, senile plaques are associated with neurotoxicity and are formed by aggregates of the β -amyloid peptide ($A\beta$), stemming from the misprocessing of the Amyloid Precursor Protein (APP) [1][2][3]. To date, the molecular mechanisms underlying AD are not completely understood. McGeer and Eikelenboom (1994) were the first to clearly identify the inflammatory component in AD, as recently confirmed by Shippey et al. (2020) [4][5][6]. Indeed, several authors pointed out the ability of $A\beta$ aggregates to activate the microglial cells, thus inducing the release of inflammatory mediators such as ROS, nitric oxide, and interleukins, all responsible for neuronal death [7][8][9][10]. Moreover, the postmortem examination of Alzheimer's patients has confirmed the incidence of high levels of pro-inflammatory cytokines, chemokines, and inflammation mediators [11].

Microglial cells play a central role in maintaining brain homeostasis and are involved in resolving inflammation from trauma or infectious microorganisms by means of phagocytosis and/or anti-inflammatory mediators. However, while the initial inflammatory response can be neuroprotective for the brain, the persistence of a challenging stimulation and the resultant strong microglia activation may turn the first line of defense (e.g., released cytokines) into detrimental and auto-toxic reactions that lead to synaptic dysfunction and neuronal cell death.

To date, no drugs used in anti-AD therapy seem to improve the prognosis. Indeed, the current therapeutic strategies are aimed at symptoms alleviation or the slowing down of disease progression. Hence, there is the need to introduce innovative drugs capable of interfering with the pathophysiological mechanisms underlying AD. In this scenario, growing interest has been focused on the endocannabinoid (eCB) system that is viewed as a pro-homeostatic and pleiotropic signaling system activated as an adaptive response to multiple pathological conditions [12][13]. The eCB system consists of cannabinoid type-1 (CB_1) and type-2 (CB_2) receptors, endogenous lipid ligands such as *N*-arachidonylethanolamine (AEA) and 2-Arachidonoylglycerol (2-AG), as well as proteins and enzymes involved in their biosynthesis and inactivation. The eCB system is also considered as part of a mechanism that may operate morphological [14], phenotypic, and functional changes of microglia and counteract the neuroinflammatory processes occurring in neurodegenerative diseases [15][16].

Studies performed both in vitro and in vivo have highlighted CB₁₋₂ receptor-mediated inhibition of A β -induced neurotoxicity, gliosis, neuroinflammation, and memory deficits [17][18][19]. Moreover, the pharmacological activation of CB₁ and/or CB₂ receptors improves memory and/or cognitive impairments in both AD-like transgenic and pharmacological (e.g., via intracerebral A β infusion) mice models [18][20][21]. In addition, the increased expression of CB₂ levels in astrocytes- and microglia-associated neuritic plaques strongly suggest a CB₂-mediated neuroprotective effect via the stimulation of microglial proliferation and migration [18][22].

In the past few years, several lines of evidence have suggested that eCB degradative enzymes could be a target for the development of anti-AD therapeutic options. Both the expression and activity of fatty acid amide hydrolase (FAAH), the enzyme responsible for AEA degradation, are increased in astrocytes and microglia-associated neuritic plaque from post-mortem AD patients' brains [17]. A reduction of AEA levels was also reported in the midfrontal and temporal cortex, where AEA levels inversely correlated with A β ₁₋₄₂ content [23]. Furthermore, the pharmacological modulation or genetic ablation of FAAH exerted different beneficial effects in terms of A β accumulation, neuroinflammation, and cognitive decline [24][25][26]. Recently, Tanaka et al., (2019) reported that the pharmacological inhibition or ablation of FAAH in BV-2 microglia cells reduced the LPS-induced release of inflammatory mediators and pro-inflammatory cytokines, and siRNA FAAH BV-2-transfected cells led to the reduced expression of pro-inflammatory genes. These findings suggest that genetic suppression and/or pharmacological inhibition of FAAH might modulate microglial phenotypes and produce anti-inflammatory effects via different mechanisms [27].

Taken together, these studies prompted us to investigate the effects produced by FAAH inactivation on microglial inflammatory processes. From among the different FAAH inhibitors developed so far, we selected the 3-(3-carbamoylphenyl)-phenyl N-cyclohexylcarbamate (URB597), as it is one of the best known compounds with a high affinity to FAAH. Hence, we assessed URB597 efficacy in terms of its ability to modulate morphological and functional changes in A β ₂₅₋₃₅-induced microglial activation in BV-2 cells. Our results show that URB597 treatment exerts a potent anti-inflammatory action by inhibiting BV-2 cell microglial polarization, by promoting cytoskeleton reorganization via cell migration and phagocytosis processes as well as by modulating the expression of pro- and anti-inflammatory markers.

2. Fatty Acid Amide Hydrolase (FAAH) Inhibition Modulates Amyloid-Beta-Induced Microglia Polarization

2.1. A β ₂₅₋₃₅ Induces Upregulation of the Iba1 Microglia Marker

Since Iba1 is a selective marker of microglial activation following nerve injury, central nervous system ischemia, inflammatory conditions, and several other forms of brain damage, we assessed whether A β ₂₅₋₃₅ could induce microglia activation by immunofluorescence and western blot analyses [28][29]. We observed an upregulation of Iba1 in BV-2 cells treated with 30 μ M of A β ₂₅₋₃₅ for 24 h, thus confirming microglial activation. URB is able to decrease A β ₂₅₋₃₅-induced microglia overactivation (Figure 1).

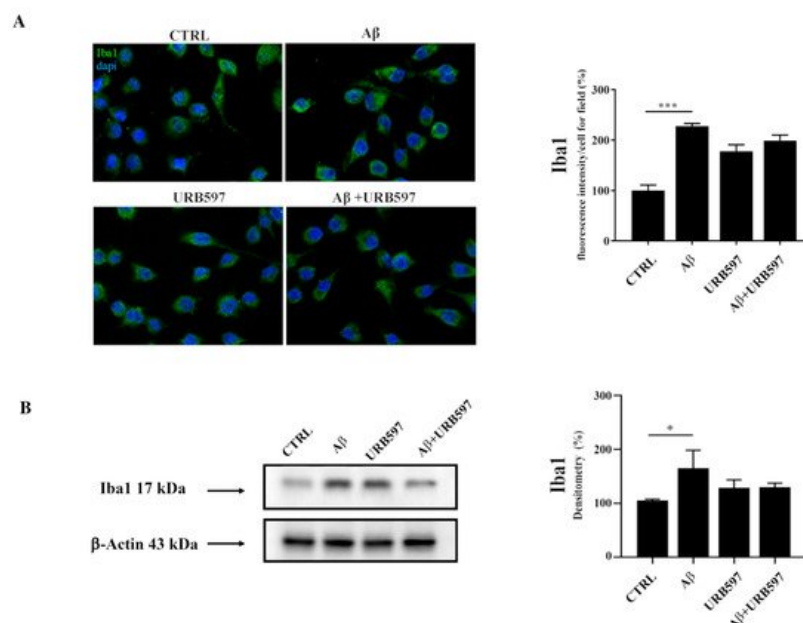


Figure 1. (A) Immunofluorescence analysis of Iba1 in BV-2 cells treated with 30 μ M A β ₂₅₋₃₅ for 24 h. Quantization of the intensity of the fluorescence signal was performed using the ImageJ software. The results are expressed as the mean \pm SD of three independent experiments. *** $p < 0.001$. Bar 20 μ m; (B) Determination of Iba1 protein levels by western blot.

The data were normalized to the β -actin signal, reported as percentage versus control (CTRL). Data are expressed as the mean \pm SEM of three independent experiments. * $p < 0.05$.

2.2. URB597 on BV-2 Cell Viability

To determine the effect of $A\beta_{25-35}$ in the presence or absence of URB597 on BV-2 cell viability, the Trypan blue assay and MTT analysis were performed. We selected 5 μ M of URB597 concentration based on the dose-response curves on BV-2 cells (data not shown). Microglia cells were pre-treated with 5 μ M URB597 and incubated with 30 μ M $A\beta_{25-35}$ for 24 h. **Figure 2A** shows a significant increase of cell death in the presence of $A\beta_{25-35}$ as compared to control cells, whereas URB597 reversed $A\beta_{25-35}$ -induced cell death. URB597 alone had no effect.

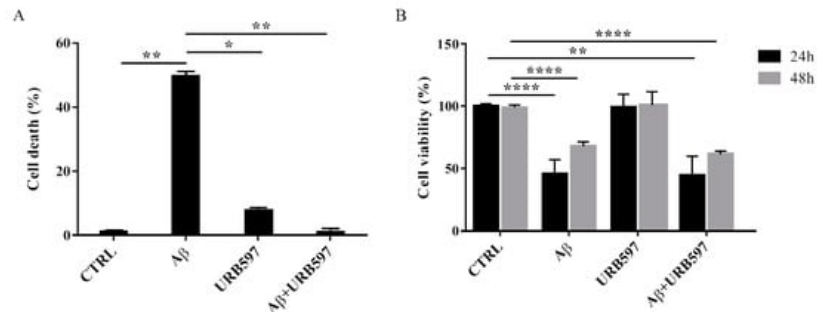


Figure 2. Effects of $A\beta_{25-35}$ in the presence or absence of URB597 on BV-2 cells. **(A)** Trypan blue exclusion test. Cell count was determined in BV-2 cells exposed for 24 h to 30 μ M of $A\beta_{25-35}$ in the presence or absence of 5 μ M of URB597 and expressed as cell death (cell death/cell death + living cell). Data are reported as percentage versus CTRL. **(B)** Analysis of cell viability was evaluated by MTT assay. MTT reduction was analyzed in the same samples of treated cells at 24 h and 48 h. Data are expressed as percentage versus CTRL. The values are the mean \pm SEM of triplicate determination from independent experiments. * $p < 0.05$, ** $p < 0.01$, *** $p < 0.0001$.

In addition, we performed an MTT assay using cells treated as described above. The data obtained show that $A\beta_{25-35}$ induced a decrease in cell viability by around 40% at 24 h, while a slight proliferative effect of $A\beta_{25-35}$ was observed at 48 h. Treatment with URB597 alone did not interfere with cell survival and did not prevent $A\beta_{25-35}$ challenge at the mitochondrial level (**Figure 2B**).

2.3. $A\beta_{25-35}$ and URB597 Effects on FAAH Enzyme Activity

Since FAAH is a selective eCB-degrading enzyme, we investigated whether $A\beta_{25-35}$ and URB597 might modulate its activity. For this purpose, BV-2 cells were pre-treated with 5 μ M URB597 for 4 h and incubated with 30 μ M $A\beta_{25-35}$ for 24 h. Notably, $A\beta_{25-35}$ induces neurotoxicity and neuroinflammation, comparable to a full-length $A\beta_{1-42}$ peptide [30].

$A\beta_{25-35}$ did not have any significant effect on FAAH activity at 24 h (**Figure 3**). URB597 was also able to inhibit FAAH activity in the presence of $A\beta_{25-35}$.

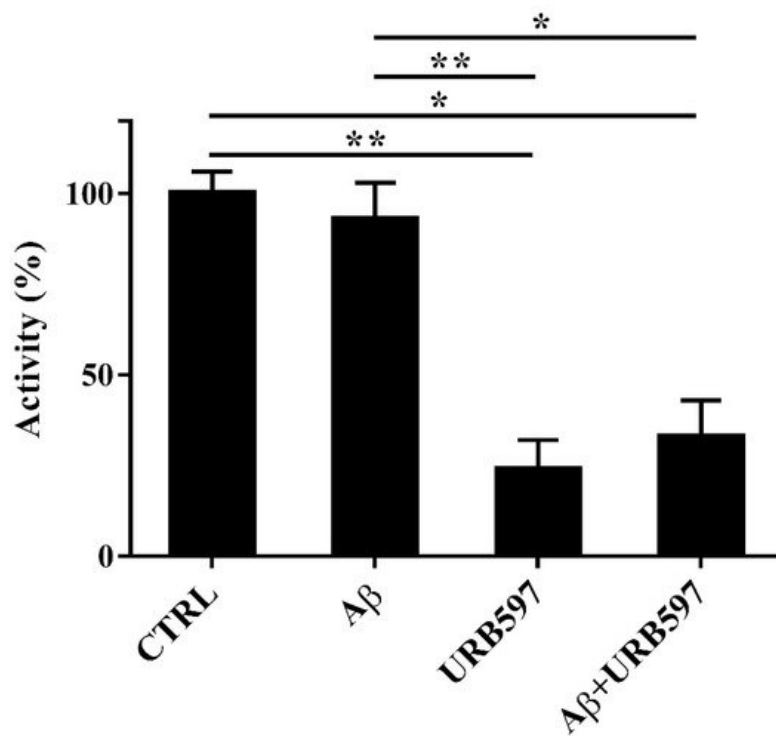


Figure 3. FAAH activity in BV-2 cells pre-treated with 5 μ M URB597 for 4 h and incubated with 30 μ M A β _{25–35} for 24 h. Data are reported as mean \pm SEM of three independent experiments. * $p < 0.05$, ** $p < 0.01$.

2.4. URB597 Reverts Morphological Changes Induced by A β _{25–35}

Microglia rapidly responds to brain injury and disease by altering its morphology and adjusting its phenotype towards an activated state. In the activated state, microglia shifts from its resting form to an ameboid form (M1/M2) [31]. Cells increase their surface area and acquire a flat morphology. To evaluate the effects of FAAH inhibition on cell morphology, we performed an immunofluorescence analysis through the phalloidin staining of F-actin on BV-2 cells pre-treated with 5 μ M of URB597 for 4 h and incubated with 30 μ M of A β _{25–35} (Figure 4). Cell morphology was analyzed at different time points (1 h, 3 h, 6 h, 24 h).

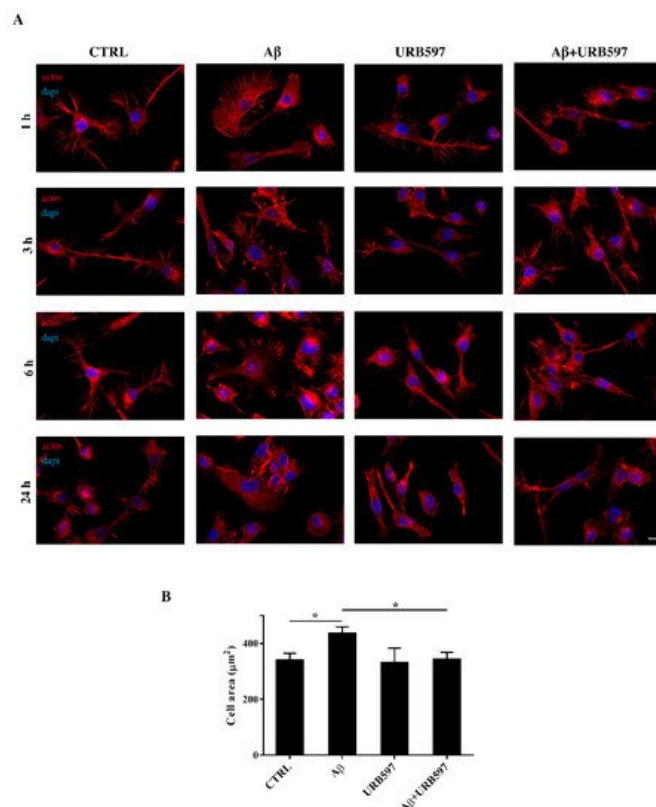


Figure 4. (A) Analysis of BV-2 cell morphology by rhodamine-conjugated phalloidin (TRITC-phalloidin) staining to highlight actin and 4', 6-diamidino-2-phenylindole (DAPI) to detect the nucleus, after pre-treatment with 5 μ M URB597 for 4 h and

incubated with 30 μM $\text{A}\beta_{25-35}$ for 1 h, 3 h, 6 h, and 24 h. **(B)** Cell areas were quantified at 24 h using Image J software. Data were reported as mean \pm SD of at least three independent experiments. * $p < 0.05$. Bar: 20 μm .

The results show that control cells exhibited a very small cell body. They had long cell ramifications and actin was organized predominantly in the filopodia, used by the cells to explore the surrounding environment. At all time-points analyzed, cells treated with $\text{A}\beta_{25-35}$ increased their surface area, acquiring a flat and polygonal morphology. Furthermore, cells retracted the branched processes that is typical of microglia in its resting form. On the other hand, cells treated with URB597 had a more rounded morphology, characterized by the shrinkage of the cellular body and the presence of several cellular processes. BV-2 cells co-treated with URB597 and $\text{A}\beta_{25-35}$, showed a phenotype similar to that obtained with only URB597 **(Figure 4A)**. These results were also confirmed by the quantitative analysis carried out by measuring the cellular area expressed in μm^2 at 24 h. The quantitative analysis confirmed that the treatment with URB597 alone produced surface areas similar to those of control cells, while after stimulation with $\text{A}\beta_{25-35}$ the cells underwent an enlargement of their soma. The cell had an area of 440 μm^2 while the control sample was at 340 μm^2 . In the combined treatment, URB597 reduced the area to values comparable to those of controls, indicating the capacity of URB597 to restore the amoeboid phenotype observed in the presence of $\text{A}\beta_{25-35}$ **(Figure 4B)**.

2.5. Effect of URB597 on Cellular Migration

One of the aspects of microglia activation is the acquisition of a migratory phenotype, which is essential for the cells to move towards the insult site. In this study, we performed a scratch assay in order to evaluate URB597-induced migratory capacity. The cells were pre-treated with 5 μM URB597 for 4 h in the presence or absence of 30 μM $\text{A}\beta_{25-35}$ for 2 h, 4 h, 6 h, and 24 h. Migration was quantified by counting the cells that migrated from the border of the scratch to the uncovered areas, and the values obtained were reported on the graph **(Figure 5B)**.

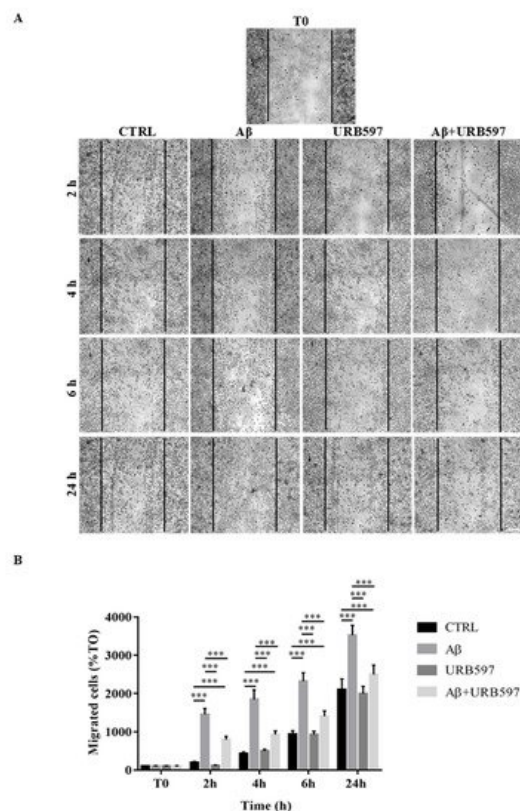


Figure 5. **(A)** Analysis of cell migration determined by scratch assay. BV-2 were pre-treated with 5 μM URB597 for 4 h in the presence or absence of 30 μM $\text{A}\beta_{25-35}$ for 2 h, 4 h, 6 h, and 24 h. T0 represents the control at time 0, and CTRL the control for each time point. **(B)** The results were normalized vs. T0 sample and re-reported as percentage. They represent the mean \pm SD of three independent experiments. *** $p < 0.001$. Bar: 200 μm .

As shown in **Figure 5**, treatment with $\text{A}\beta_{25-35}$ induced migration just 2 h after stimulation, as compared to the control cells. We demonstrated that URB597 alone did not affect cell migration, and that URB597 pre-treatment reduced BV-2 migration induced by $\text{A}\beta_{25-35}$. The migratory effect was directly proportional to the number of incubation hours.

2.6. URB597 Increases Microglia Phagocytic Capacity

To determine whether URB597 has a role in phagocytosis, we assessed FITC-dextran microglial uptake. BV-2 cells pre-treated with 5 μ M URB597 for 4 h and incubated with 30 μ M A β_{25-35} for 24 h were incubated for 1 h with FITC-dextran and analyzed by a microscope; the fluorescence images are shown in **Figure 6A**. As shown in **Figure 6B**, we evaluated the intensity of the fluorescent dextran in the different treatments. BV-2 cells treated with A β_{25-35} showed a reduced ability to absorb dextran compared to untreated cells. The sample treated only with URB597 showed an intensity value comparable to that obtained by IL-10 stimulation. In the combined treatment with A β_{25-35} and URB597, the inhibitor turned out to be capable of increasing the intensity value as compared to the A β_{25-35} sample. LPS and IL-10 were used as reference compounds that could reduce [32] or increase phagocytosis [33][34]. Moreover, the number of dextran-positive cells was quantified on the total cells and the results were reported as percentage (**Figure 6C**). After stimulation with A β_{25-35} as well as with LPS, the number of dextran-positive cells was reduced by approximately 80% relative to the control cells. On the other hand, treatment with URB597 alone showed values similar as the control but lower if compared to the IL-10 treated sample. In the A β_{25-35} and URB597 combined treatment, the inhibitor improved the number of dextran-positive cells, with higher values of phagocytic cells as compared with the A β_{25-35} treated sample.

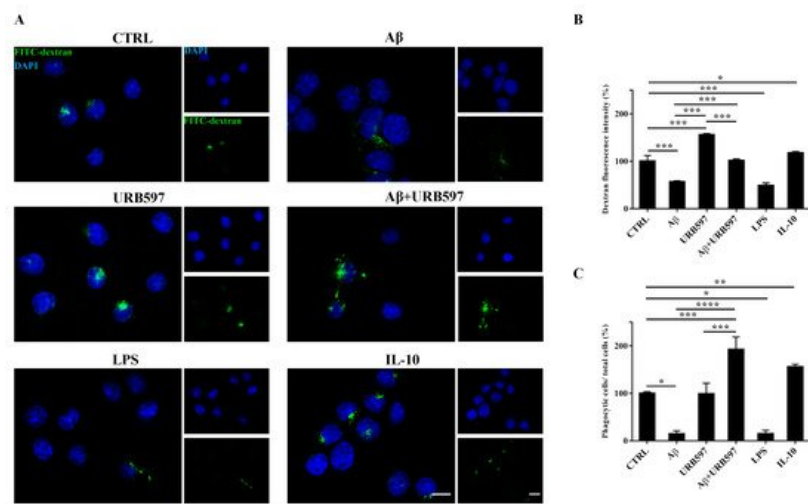


Figure 6. Analysis of the phagocytosis process using FITC-dextran on BV-2 cells pre-treated with 5 μ M URB597 and incubated with 30 μ M A β_{25-35} for 24 h. **(A)** Representative immunofluorescence images of FITC-dextran uptake. **(B)** Quantization of the intensity of FITC-dextran. **(C)** Quantization of the number of dextran-positive cells on the total cells. The data were normalized to CTRL and reported as a percentage. The results were expressed as the mean \pm SD of three independent experiments. Statistical significance was determined using ANOVA analysis by Tukey's test. * $p < 0.05$, ** $p < 0.01$, *** $p < 0.001$, **** $p < 0.0001$. Bar: 20 μ m.

2.7. URB597 Affects Rho GTPases Activity

Cytoskeleton plasticity and the formation of actin-rich structures, with consequent morphological modifications, are regulated by the Rho GTPase protein family. Since the Rho GTPase family is a master regulator of cytoskeletal reorganization and plays an important role in membrane trafficking [35][36], we investigated whether the Rho and Cdc42, components of the Rho GTPase family, were able to regulate the different activated states of microglia cells. To evaluate the influence of the FAAH inhibitor on this class of proteins, we performed pull-down analyses on the total protein extraction from BV-2 cells pre-treated with 5 μ M URB597 for 4 h and incubated with 30 μ M A β_{25-35} for 24 h. We examined RhoA, which is involved in the assembly of contractile actin, and Cdc42 proteins that is involved in filopodia formation.

This analysis allows for the precipitation of active GTPases proteins through a specific binding protein. Our results show a marked increase of RhoA activity in the samples treated with A β_{25-35} as compared to control cells, whereas a decrease was observed in the URB597-treated samples with respect to A β_{25-35} samples (**Figure 7A**). As shown in **Figure 7B**, Cdc42 activity significantly increased in samples treated with URB597, considering both against A β_{25-35} and control cells samples.

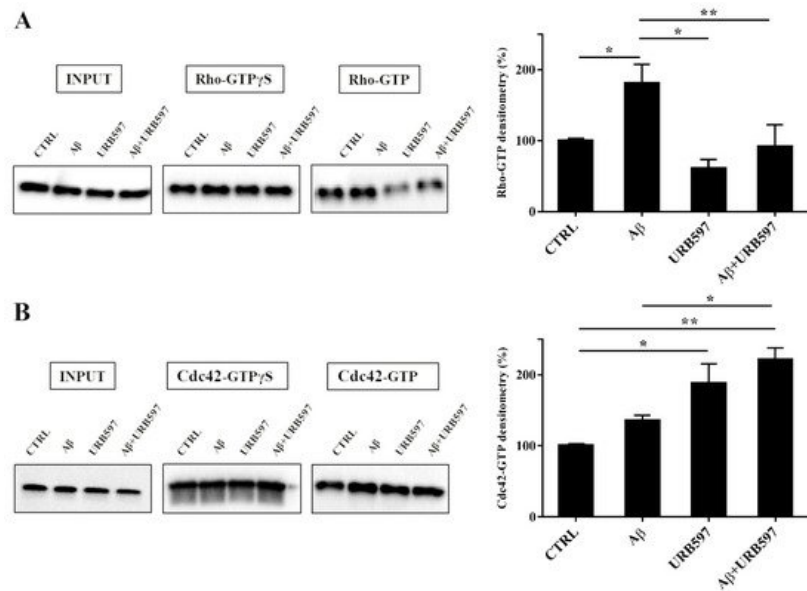


Figure 7. Pull-down assay of Rho and Cdc42 proteins (A,B). BV-2 cells were pre-treated with 5 μ M URB597 for 4 h and incubated with 30 μ M A β _{25–35} for 24 h. The pull-down assay with GTP γ S was used as positive control. The results are reported as a percentage versus control (CTRL). Densitometric analyses were performed with ImageLab software (Biorad) and normalized to INPUT. * $p < 0.05$, ** $p < 0.01$.

2.8. URB597 Reduces mRNA IL-1 β and TNF- α Expression, Increases TGF- β and IL-10 Expression

The activation of Rho GTPases supports the hypothesis of A β -driven cytoskeleton rearrangement, ultimately leading to an increase of migration and a reduction of phagocytosis. Since these effects were counteracted by URB597, we aimed at determining the level of inflammation in our BV-2 cell model.

The expression of pro-inflammatory cytokines such as IL-1 β and TNF- α as well as anti-inflammatory cytokines such as TGF- β and IL-10, were analyzed by qPCR. BV-2 cells were pre-treated with 5 μ M URB597 for 4 h and incubated with 30 μ M A β _{25–35} for 1 h and 24 h. The results presented in **Figure 8A,B** demonstrate that IL-1 β and TNF- α expressions increased within 1 h in BV-2 cells treated with A β _{25–35} as compared to the control. On the contrary, a reduction of cytokines was observed in the sample with the combined treatment as compared to A β _{25–35} alone. No changes were detected for IL-1 β and TNF- α levels in BV-2 cells incubated with 30 μ M A β _{25–35} for 24 h. We also observed that treatment with A β _{25–35} did not modify TGF- β expression, while URB597 alone or in combination with A β _{25–35} upregulated TGF- β at 24 h, as shown in **Figure 8C**.

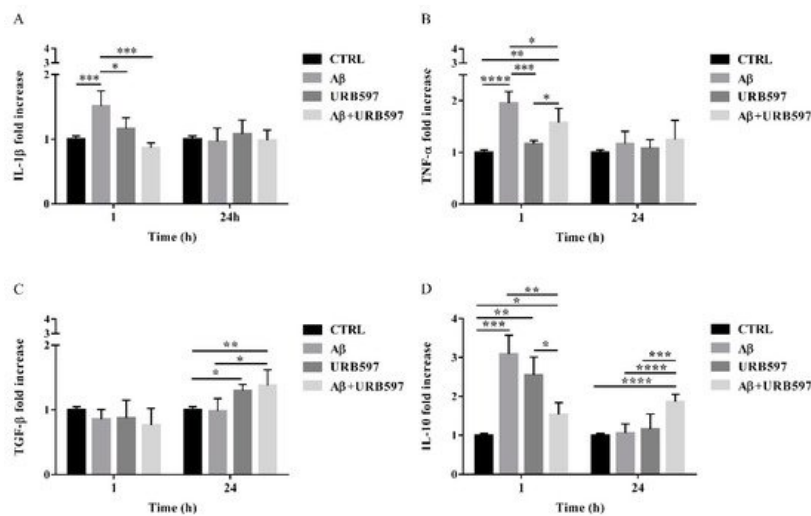


Figure 8. The mRNA expression of different inflammatory cytokines such as IL-1 β (A), TNF- α (B), TGF- β (C), and IL-10 (D), monitored by qPCR and normalized to 18S ribosome subunit. Data are shown as mean \pm SD from three independent experiments performed in triplicate. Expression profiles were determined using the 2- $\Delta\Delta$ CT method. * $p < 0.05$, ** $p < 0.01$, *** $p < 0.001$, **** $p < 0.0001$.

Moreover, both A β _{25–35} and URB597 administration, alone or in combination, induced an increase of IL-10 expression within 1 h, while after 24 h of stimulation the effect was persistent only in the A β _{25–35} and URB597 combined treatment

(Figure 8D).

2.9. URB597 Modulates Both iNOS and Arg-1 Expression

The activation of microglia is a polarized process that can lead either to the potentially neurotoxic M1-activated phenotype or to the neuroprotective M2-activated phenotype [32]. To evaluate the M1 or M2 states in the treated cells, we performed both immunofluorescence and RT-qPCR analyses and assessed the level of nitric oxide synthase (iNOS) and Arginase-1 (Arg-1), which are markers of the M1 and M2 microglia phenotypes, respectively (Figure 9). BV-2 cells were pre-treated with 5 μ M URB597 for 4 h and incubated with 30 μ M A β _{25–35} for 24 h. LPS and IL-4 were considered as positive controls for iNOS and Arg-1 markers, respectively. As shown in Figure 9A–D, the stimulation of BV-2 cells with A β _{25–35} induced a significant enhancement of iNOS, whereas a reduction of Arg-1 was observed in comparison to control. The combination of URB597 and A β _{25–35} induced a decrease in iNOS expression and an increase in Arg-1 with respect to A β _{25–35}. URB597 alone did not affect the expression of both markers.

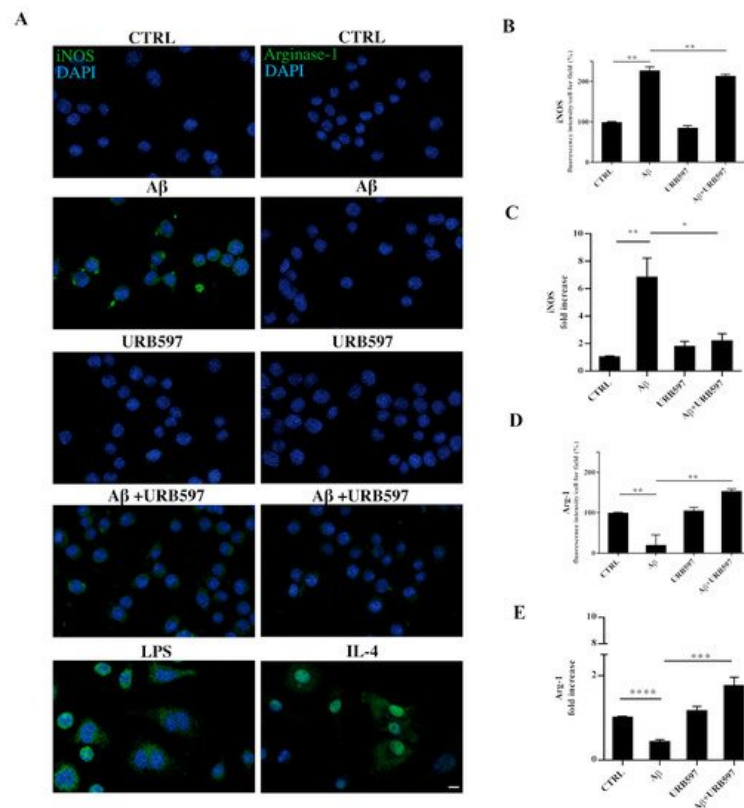


Figure 9. BV-2 cells were pre-treated with URB597 5 μ M for 4 h and incubated with A β _{25–35} 30 μ M for 24 h. LPS and IL-4 were used as positive controls for iNOS and Arg-1 markers, respectively. Representative immunofluorescence images of iNOS and Arg-1 (A). Quantitative immunofluorescence analysis of iNOS (B) and Arg-1 (D). Quantification of fluorescence signal intensity was analyzed using ImageJ software. The results are expressed as the mean \pm SD of three independent experiments. ** $p < 0.01$. Bar 20 μ m. iNOS (C) and Arg-1 (E) mRNA expressions were evaluated by qRT-PCR at 24 h. Data are shown as mean \pm SD from three independent experiments performed in triplicate. Expression profiles were determined using the 2- $\Delta\Delta$ CT method. * $p < 0.05$, ** $p < 0.01$, *** $p < 0.001$, **** $p < 0.0001$.

References

1. Mayeux, R.; Sano, M. Treatment of Alzheimer's disease. *N. Engl. J. Med.* 1999, 341, 1670–1679.
2. Walsh, D.M.; Selkoe, D.J. A beta oligomers—A decade of discovery. *J. Neurochem.* 2007, 101, 1172–1184.
3. Yankner, B.A. New clues to Alzheimer's disease: Unraveling the roles of amyloid and tau. *Nat. Med.* 1996, 2, 850–852.
4. Eikelenboom, P.; Zhan, S.S.; van Gool, W.A.; Allsop, D. Inflammatory mechanisms in Alzheimer's disease. *Trends Pharmacol. Sci.* 1994, 15, 447–450.
5. McGeer, P.L.; Rogers, J.; McGeer, E.G. Neuroimmune mechanisms in Alzheimer disease pathogenesis. *Alzheimer Dis. Assoc. Disord.* 1994, 8, 149–158.
6. Shippy, D.C.; Ulland, T.K. Microglial Immunometabolism in Alzheimer's Disease. *Front. Cell. Neurosci.* 2020, 14, 563446.

7. Akiyama, H.; Arai, T.; Kondo, H.; Tanno, E.; Haga, C.; Ikeda, K. Cell mediators of inflammation in the Alzheimer disease brain. *Alzheimer Dis. Assoc. Disord.* 2000, 14 (Suppl. 1), S47–S53.
8. Davalos, D.; Grutzendler, J.; Yang, G.; Kim, J.V.; Zuo, Y.; Jung, S.; Littman, D.R.; Dustin, M.L.; Gan, W.B. ATP mediates rapid microglial response to local brain injury in vivo. *Nat. Neurosci.* 2005, 8, 752–758.
9. Kitazawa, M.; Yamasaki, T.R.; LaFerla, F.M. Microglia as a potential bridge between the amyloid beta-peptide and tau. *Ann. N. Y. Acad. Sci.* 2004, 1035, 85–103.
10. Rogers, J.; Strohmeier, R.; Kovelowski, C.J.; Li, R. Microglia and inflammatory mechanisms in the clearance of amyloid beta peptide. *Glia* 2002, 40, 260–269.
11. Perry, G.; Cash, A.D.; Smith, M.A. Alzheimer Disease and Oxidative Stress. *J. Biomed. Biotechnol.* 2002, 2, 120–123.
12. Friedman, D.; French, J.A.; Maccarrone, M. Safety, efficacy, and mechanisms of action of cannabinoids in neurological disorders. *Lancet Neurol.* 2019, 18, 504–512.
13. Cristino, L.; Bisogno, T.; Di Marzo, V. Cannabinoids and the expanded endocannabinoid system in neurological disorders. *Nat. Rev. Neurol.* 2020, 16, 9–29.
14. Malorni, W.; Bari, M.; Straface, E.; Battista, N.; Matarrese, P.; Finazzi-Agro, A.; Del Principe, D.; Maccarrone, M. Morphological evidence that 2-arachidonoylglycerol is a true agonist of human platelets. *Thromb. Haemost.* 2004, 92, 1159–1161.
15. Fezza, F.; Bari, M.; Florio, R.; Talamonti, E.; Feole, M.; Maccarrone, M. Endocannabinoids, related compounds and their metabolic routes. *Molecules* 2014, 19, 17078–17106.
16. Jackson, S.J.; Diemel, L.T.; Pryce, G.; Baker, D. Cannabinoids and neuroprotection in CNS inflammatory disease. *J. Neurol. Sci.* 2005, 233, 21–25.
17. Benito, C.; Nunez, E.; Tolon, R.M.; Carrier, E.J.; Rabano, A.; Hillard, C.J.; Romero, J. Cannabinoid CB2 receptors and fatty acid amide hydrolase are selectively overexpressed in neuritic plaque-associated glia in Alzheimer's disease brain. *J. Neurosci.* 2003, 23, 11136–11141.
18. Ramirez, B.G.; Blazquez, C.; Gomez del Pulgar, T.; Guzman, M.; de Ceballos, M.L. Prevention of Alzheimer's disease pathology by cannabinoids: Neuroprotection mediated by blockade of microglial activation. *J. Neurosci.* 2005, 25, 1904–1913.
19. Maccarrone, M.; Totaro, A.; Leuti, A.; Giacobuzzo, G.; Scipioni, L.; Mango, D.; Coccorello, R.; Nistico, R.; Oddi, S. Early alteration of distribution and activity of hippocampal type-1 cannabinoid receptor in Alzheimer's disease-like mice overexpressing the human mutant amyloid precursor protein. *Pharmacol. Res.* 2018, 130, 366–373.
20. Aso, E.; Juves, S.; Maldonado, R.; Ferrer, I. CB2 cannabinoid receptor agonist ameliorates Alzheimer-like phenotype in AbetaPP/PS1 mice. *J. Alzheimers Dis.* 2013, 35, 847–858.
21. Martin-Moreno, A.M.; Brera, B.; Spuch, C.; Carro, E.; Garcia-Garcia, L.; Delgado, M.; Pozo, M.A.; Innamorato, N.G.; Cuadrado, A.; de Ceballos, M.L. Prolonged oral cannabinoid administration prevents neuroinflammation, lowers beta-amyloid levels and improves cognitive performance in Tg APP 2576 mice. *J. Neuroinflamm.* 2012, 9, 8.
22. Walter, L.; Stella, N. Cannabinoids and neuroinflammation. *Br. J. Pharmacol.* 2004, 141, 775–785.
23. Jung, K.M.; Astarita, G.; Yasar, S.; Vasilevko, V.; Cribbs, D.H.; Head, E.; Cotman, C.W.; Piomelli, D. An amyloid beta42-dependent deficit in anandamide mobilization is associated with cognitive dysfunction in Alzheimer's disease. *Neurobiol. Aging* 2012, 33, 1522–1532.
24. Chen, H.C.; Spiers, J.G.; Sernia, C.; Lavidis, N.A. Inhibition of Fatty Acid Amide Hydrolase by PF-3845 Alleviates the Nitrergic and Proinflammatory Response in Rat Hippocampus Following Acute Stress. *Int. J. Neuropsychopharmacol.* 2018, 21, 786–795.
25. Piro, J.R.; Benjamin, D.I.; Duerr, J.M.; Pi, Y.; Gonzales, C.; Wood, K.M.; Schwartz, J.W.; Nomura, D.K.; Samad, T.A. A dysregulated endocannabinoid-eicosanoid network supports pathogenesis in a mouse model of Alzheimer's disease. *Cell Rep.* 2012, 1, 617–623.
26. Vazquez, C.; Tolon, R.M.; Grande, M.T.; Caraza, M.; Moreno, M.; Koester, E.C.; Villaescusa, B.; Ruiz-Valdepenas, L.; Fernandez-Sanchez, F.J.; Cravatt, B.F.; et al. Endocannabinoid regulation of amyloid-induced neuroinflammation. *Neurobiol. Aging* 2015, 36, 3008–3019.
27. Tanaka, M.; Yagyu, K.; Sackett, S.; Zhang, Y. Anti-Inflammatory Effects by Pharmacological Inhibition or Knockdown of Fatty Acid Amide Hydrolase in BV2 Microglial Cells. *Cells* 2019, 8, 491.
28. Harry, G.J. Microglia during development and aging. *Pharmacol. Ther.* 2013, 139, 313–326.
29. Mori, I.; Imai, Y.; Kohsaka, S.; Kimura, Y. Upregulated expression of Iba1 molecules in the central nervous system of mice in response to neurovirulent influenza A virus infection. *Microbiol. Immunol.* 2000, 44, 729–735.

30. Frozza, R.L.; Horn, A.P.; Hoppe, J.B.; Simao, F.; Gerhardt, D.; Comiran, R.A.; Salbego, C.G. A comparative study of beta-amyloid peptides Abeta1-42 and Abeta25-35 toxicity in organotypic hippocampal slice cultures. *Neurochem. Res.* 2009, 34, 295–303.
31. Lucin, K.M.; Wyss-Coray, T. Immune activation in brain aging and neurodegeneration: Too much or too little? *Neuron* 2009, 64, 110–122.
32. Yunna, C.; Mengru, H.; Lei, W.; Weidong, C. Macrophage M1/M2 polarization. *Eur. J. Pharmacol.* 2020, 877, 173090.
33. Francos-Quijorna, I.; Amo-Aparicio, J.; Martinez-Muriana, A.; Lopez-Vales, R. IL-4 drives microglia and macrophages toward a phenotype conducive for tissue repair and functional recovery after spinal cord injury. *Glia* 2016, 64, 2079–2092.
34. Gordon, S.; Taylor, P.R. Monocyte and macrophage heterogeneity. *Nat. Rev. Immunol.* 2005, 5, 953–964.
35. Ridley, A.J. Rho GTPases and actin dynamics in membrane protrusions and vesicle trafficking. *Trends Cell Biol.* 2006, 16, 522–529.
36. Stankiewicz, T.R.; Linseman, D.A. Rho family GTPases: Key players in neuronal development, neuronal survival, and neurodegeneration. *Front. Cell. Neurosci.* 2014, 8, 314.
37. Orihuela, R.; McPherson, C.A.; Harry, G.J. Microglial M1/M2 polarization and metabolic states. *Br. J. Pharmacol.* 2016, 173, 649–665.

Retrieved from <https://encyclopedia.pub/entry/history/show/29733>